Journal of Polymers and the Environment
https://doi.org/10.1007/s10924-024-03216-6

ORIGINAL PAPER

Assessment of Lignin Residues from Bioethanol Production of Olive Stones as Green Chemical Thickener of Epoxidized Linseed Oil

E. Cortés-Triviño[1] · C. Valencia[1] · J. M. Franco[1] · J. M. Oliva[2] · P. Manzanares[2] · M. E. Eugenio[3] · D. Ibarra[3]

Accepted: 14 February 2024

Abstract

This work focused on the characterization of lignin residues from bioethanol production of olive stones (OS) and the use of these residues to chemically thicken epoxidized linseed oil (ELO). OS were processed by an acid/steam explosion pretreatment, followed by pre-saccharification, using different enzyme dosages, and simultaneous saccharification and fermentation. The chemical composition of the OS lignin residues was analysed, revealing a high lignin content (66.6–69.5%), and lower quantities of glucan (17.4–19.3%) and xylan (2.8–2.9%). Whereas, the structural properties of OS lignin residues were characterized by Fourier-transform infrared (FTIR) spectroscopy, nuclear magnetic resonance (NMR), thermogravimetric analysis and size exclusion chromatography (SEC). OS lignin residues displayed the main inter-unit linkages (β–β′ resinol (51.0–59.0%), followed by β-O-4′ alkyl aryl ethers (27.0–35.2%) and β-5′ phenylcoumaran (11.4–13.2%) substructures), high molecular weights (22,000–25900 Da), low S/G ratios (1.2–1.5) and phenolic groups content (48–55 mg GAE/g lignin). Moreover, OS lignin residues were dispersed in ELO to obtain thickened formulations, which were characterized by FTIR and NMR. Oil thickening was achieved by promoting the chemical crosslinking between lignocellulose hydroxyl groups and ELO epoxy groups, enabling the compatibilization of both components. Up to tenfold viscosity increment of the resulting thickened formulations in relation to ELO's viscosity was observed. Besides, thickened formulations exhibited viscoelastic properties, evincing oil structuration to some extent.

✉ M. E. Eugenio
mariaeugenia@inia.csic.es

✉ D. Ibarra
ibarra.david@inia.csic.es

[1] Pro2TecS – Chemical Process and Product Technology Research Center, ETSI, Departamento de Ingeniería Química, Campus de "El Carmen", Universidad de Huelva, 21071 Huelva, Spain

[2] Advanced Biofuels and Bioproducts Unit, Department of Energy, CIEMAT, Avda. Complutense 40, 28040 Madrid, Spain

[3] Instituto de Ciencias Forestales (INIA, CSIC), Ctra de la Coruña Km 7.5, 28040 Madrid, Spain

Published online: 09 April 2024

Graphical Abstract

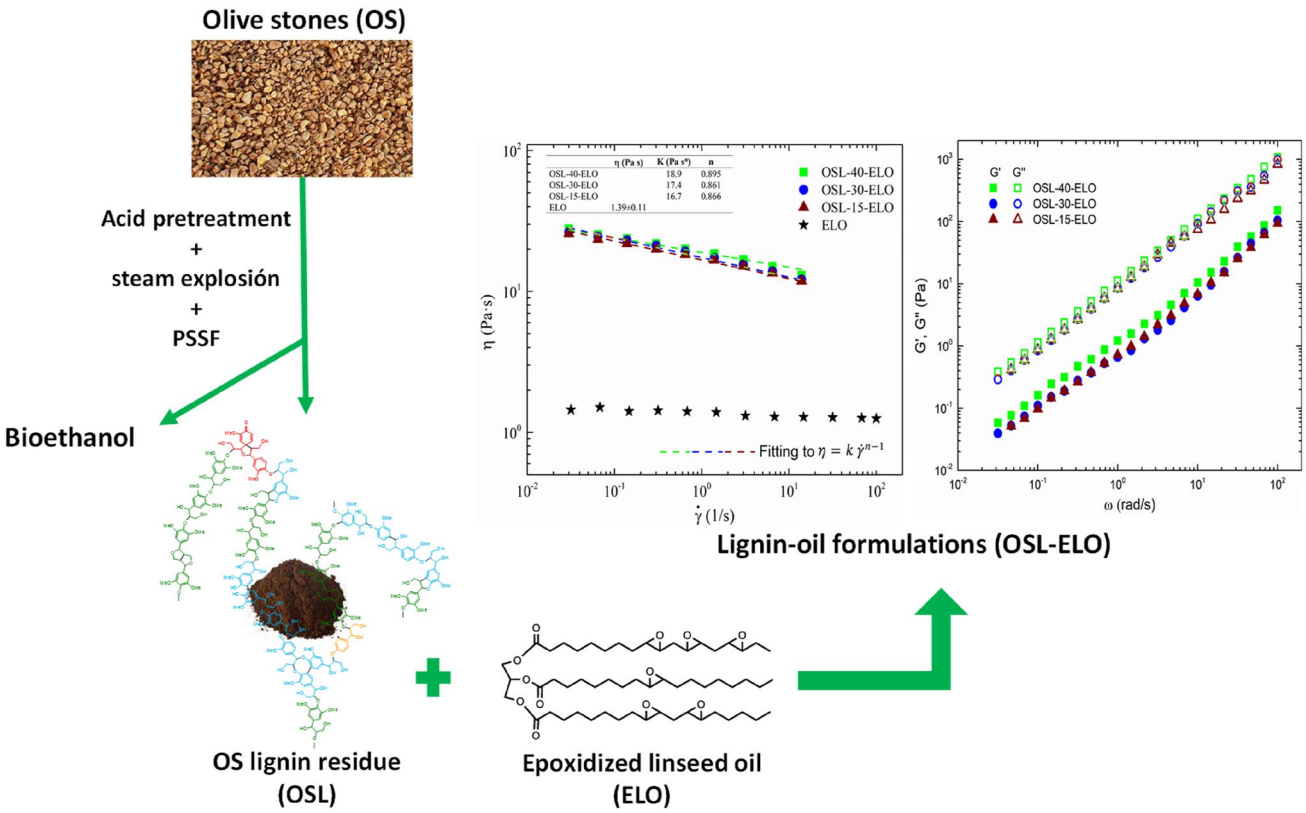

Keywords Epoxidized vegetable oil · Green thickener · Intrinsic viscosity · Lignin characterization · Lignin residue · Olive stones

Introduction

Nowadays, the transition from fossil fuels to renewable sources is a critical and ongoing process aimed at reducing our reliance on limited and environmentally detrimental resources. This transition is motivated by the need to mitigate climate change resulting from the increasing accumulation of greenhouse gases in the atmosphere. Just in 2020, a staggering 31.5Gt of CO_2 were emitted worldwide, with the transportation sector accounting for a significant portion of 23% of these emissions [1]. Similarly, in Europe, CO_2 emissions amounted to 2.5 Gt with the transport sector contributing at 24.6% [2]. Due to these circumstances and considering the great potential of biomass as renewable energy resources, numerous technologies have been successfully devised to convert biomass into biofuels, being both biodiesel and bioethanol the predominant biofuels widely used in the global transportation sector [3]. Particularly, while bioethanol can be derived from a range of organic sources including biomass, agricultural crops, and industrial wastes, the primary focus of its production has been centered on food crops such as starchy and sugary crops. Nevertheless, in recent years, there has been a growing emphasis on utilizing lignocellulosic biomass to produce bioethanol, offering notable economic and environmental benefits compared to relying on the above mentioned food crops [4, 5]. In this sense, agriculture and forestry wastes, as well as residues from agro-food industries, hold a significant potential as lignocellulosic source to produce biofuels since they offer several advantages, including their widespread availability, cost-effectiveness, and the need for appropriate disposal methods in many cases.

Within this framework, olive stone (OS) residues, which are the leftover materials from the processing of olives for oil production, can be valorised as raw material to produce bioethanol. These byproducts consist of the olive pits, skins, and some fragments of the pulp and have potential as a renewable feedstock due to their composition, great availability, renewability, and low-cost, which turn them into an attractive option for sustainable utilization in many applications. Only in Spain, over 600,000 tons of OS are generated annually, with more than 80% being utilized for energy

applications and heat generation. However, there is still a surplus of this by-product, which can be effectively utilized as a sustainable raw material, thereby fostering the principles of circular economy and contributing to both waste reduction and environmental stewardship [6, 7].

Olive stones, like other lignocellulosic feedstocks, consist primarily of cellulose, hemicellulose and lignin as major components, which are forming a complex and resistant structure within the plant cell walls. In the process of converting lignocellulosic biomass to ethanol, on the one hand the fermentable sugars present in the material, in the form of cellulose and hemicellulose, are released through a pretreatment and enzymatic hydrolysis step [8]. On the other hand, a side-stream residue enriched in lignin, which is often utilized as a solid fuel in the facility to generate energy for the overall process, is obtained. Lignin possesses distinct characteristics than carbohydrates, including an aromatic structure, hydrophobicity, and a high concentration of reactive groups, among others, which turn it in a compelling precursor for the production of high-value chemicals and materials [9]. It is composed of three distinct 4-hydroxyphenylpropanoid units that are interconnected through various ether and C–C linkages [10]. Among them, β-aryl ether linkages (β-O-4′) constitute the most abundant bond, followed by C–C linkages such as resinol (β–β′) and phenylcoumaran (β-5′), among others. A comprehensive elucidation of the structural characteristics and properties of lignins is crucial in determining the most effective approach for their valorization. These features and properties are influenced by factors such as the type of lignocellulosic material and the isolation process employed [11]. Currently, the majority (over 90%) of global lignin production originates from the pulp and paper industry, specifically through kraft and sulphite pulping processes [12]. As we move towards 2030, the full-scale operation of second-generation biorefineries is anticipated to result in an increase in lignin production. Therefore, gaining a deeper understanding of these aspects is imperative to identify the optimal strategy for lignin utilization and valorization.

Among the functional groups in the chemical structure of lignin, hydroxyl groups are highly desirable chemical sites to promote further reactions due to their high reactivity with other multiple chemical groups like amines, epoxides, isocyanate groups, etc., [13]. Many authors have focused their research on the chemical modification of lignin through these hydroxyl groups to increase the reactivity of these residues, with the aim of valorizing and turning them into promising alternatives to be employed as sustainable raw materials for diverse applications. For instance, lignocellulosic materials and vegetable oils have been combined in industrially relevant products such as lubricants, adhesives, or coatings, among others [14–17], aiming to find new environmentally friendly alternatives to replace the commercial fossil fuel-based products available on the market today. This shift towards renewable and biodegradable resources is driven by the desire to foster sustainability and reduce the environmental impact associated with conventional consumer goods and industrial products [18, 19]. In this regard, vegetable oils and their derivatives [20], as well as natural polymers [21–23], are nowadays in demand to produce sustainable formulations with diverse functional properties depending on their application. However, in spite of the numerous advantages displayed by these feedstocks, they cannot be directly employed together to develop outstanding formulations due to their chemical incompatibility and different polarities [24], being essential to subject them to chemical modifications in order to improve the compatibilization among the components and ultimate properties [25, 26]. In particular, epoxidation of either vegetable oils or lignocellulosic materials has emerged as a promising chemical route for enhancing compatibility between these two bioresources. For instance, this approach allows the production of thickened oil-based formulations with outstanding rheological properties, making them well-suited for lubricating applications, among others [16, 17, 27]. Thus, epoxidized vegetable oils have been widely studied in recent years as feedstock for different industrial products [28, 29], since they show excellent lubricity properties, biodegradable characteristics, and high reactivity with several chemical groups by means of nucleophilic attack to the oxirane rings. Traditionally, grafting epoxy rings onto fatty acid chains in various vegetable oils has been achieved across their double bonds [30, 31]. However, nowadays there are commercially available options, with epoxidized linseed oil being among the available choices, which present an intriguing pathway worth of exploring for these purposes.

Within this framework, this study focuses on exploring novel valorization pathways for lignin residues derived from the bioethanol production of olive stones (hereinafter OS lignin residues), aiming at (i) providing a comprehensive chemical characterization of these residues, (ii) promoting the chemical interaction of the OS lignin residues and epoxidized linseed oil to achieve a thickening effect and, as a result, (iii) producing sustainable, high value-added and versatile vegetable oil-based formulations with enhanced rheological properties for application in a variety of fields where the viscosity modulation is relevant in product performance, e.g. as bio-based lubricants, or adhesive and coatings precursors.

Materials and Methods

Raw Material

Olive stones (OS) (8% moisture content and particle size ranging 1–3 mm) were supplied by a local industry in Jaén (Andalusia, Spain). OS composition was (dry weight basis):

20.9% cellulose, 26.0% hemicelluloses, 35.6% lignin, 6.3% extractives, 0.6% ash, and 5.9% acetyl groups [32]. Epoxidized linseed oil (ELO), containing more than 8 wt% of oxirane oxygen, was supplied by Traquisa S.L. (Barcelona, Spain). More information about its composition has been included in Table S1.

Procedures for Obtaining OS Lignin Residues

Pretreatment

OS were subjected to a two-step pretreatment, including acid pretreatment in a Parr reactor (10.5 g H_2SO_4/100 g OS for 60 min at 128 °C), followed by steam explosion (SE) at 195 °C for 5 min, as described by Padilla-Rascón et al. [32]. Briefly, in the first pretreatment step (diluted acid sulphuric), OS biomass was pretreated in the reactor with a solid/liquid ratio of 33% (w/v). The resulting slurry after acid pretreatment, was filtered to separate the liquid (hemicellulosic sugars-containing liquor) and an insoluble solid that, without washing, was used to feed the steam explosion reactor. The moisture content of this solid used as feedstock was 40%. The slurry generated after SE, having a solid/liquid ratio of close to 1/1, was filtered to separate again the liquid (liquor) and a water insoluble solid (WIS) fraction. WIS fraction was used as substrate for ethanol production in a presaccharification and simultaneous saccharification and fermentation (PSSF) process. The main WIS components were (dry weight basis): 35.4% cellulose, 2.6% hemicellulose, and 57.5% lignin.

Presaccarification and Simultaneous Saccharification and Fermentation (PSSF) Process

PSSF was carried out in a two-step procedure. Firstly, a presaccharification step was carried out by incubating the WIS fraction samples at 20% (w/w) concentration with 1.5 kg of 0.05 M sodium citrate buffer (pH 4.8) in a bioreactor of 15 L capacity (Terrafors-IS, Infors HT, Switzerland), at 50 °C for 24 h. Enzyme doses of 15, 30 or 40 FPU of Cellic® CTec2/g of dry substrate (Novozymes A/S, Bagsværd, Denmark) were tested. After the presaccharification, 0.5 kg of the incubated materials were transferred to 1 L Erlenmeyer flasks to undergo the simultaneous saccharification and fermentation (SSF) stage and to this end, the temperature was reduced to 35 °C. Salts were added at the following concentrations (in g/L): yeast extract (2), NH_4Cl (1), KH_2PO_4 (1), $MgSO_4{\cdot}7H_2O$ (0.3), and the flasks were inoculated with 1 g/L of *Saccharomyces cerevisiae* ("Ethanol Red", Fermentis, France). SSF was run by triplicate in an orbital shaker at 150 rpm for 48 h. Then, the fermentation broth, having an ethanol concentration of 36 g L^{-1},was filtered and the insoluble solids were rinsed with abundant water to obtain the OS lignin residues. The final PSSF yield obtained was 65% of theoretical, considering the glucose that would be available for hydrolysis and fermentation in the WIS fraction used as substrate (cellulose content of WIS). These OS lignin samples have been denoted according to the hydrolytic enzyme (Cellic® CTec2) dose used during presaccharification as OSL-40 (OS lignin residue when 40 FPU/g of the dry substrate is used), OSL-30 (OS lignin residue when 30 FPU/g of the dry substrate is used), and OSL-15 (OS lignin residue when 15 FPU/g of the dry substrate is used).

Dispersion of OS Lignin Residues in Epoxidized Linseed Oil

OS lignin residues were subjected first to a pre-milling step in a mortar to favour their dispersion in the oil medium. Afterwards, both raw materials were mixed (30 wt% OS lignin concentration) in an open vessel, at room temperature for 24 h, by using a controlled-rotational speed (70 rpm) mixing device (RW 20, Ika), equipped with an anchor impeller. A quaternary ammonium salt (tetrabutylammonium bromide, TBAB) was also added as a catalyst (1 wt%). A final curing stage was applied by placing the mixtures in an oven at 150 °C for 2 h. Finally, samples were subjected to a homogenization treatment (10,000 rpm for 1 min), using an Ultra-Turrax T-25 (Ika) rotor–stator turbine. Formulations obtained from the dispersion of the OS lignin residues OSL-40, OSL-30, and OSL-15 in ELO were named as OSL-40-ELO, OSL-30-ELO, and OSL-15-ELO, respectively.

Analytical Methods

The chemical composition of OS lignin residues (OSL-40, OSL-30, and OSL-15) was examined according to the methods described by the National Renewable Energies Laboratory [33], using the protocol NREL/TP-510-42618.

The total phenolic groupss content of OS lignin residues was measured according to Folin–Ciocalteau method [34]. Absorbances were measured at 760 nm using a UV–Vis spectrophotometer (Lambda 365, PerkinElmer, Boston, MA, USA). A calibration curve of a standard solution of gallic acid was used to quantify the total phenolic groups content [expressed as mg gallic acid equivalent (GAE)/g of lignin (on a dry basis)].

Fourier Transform Infrared (FTIR) Spectroscopy Analysis

FTIR spectra were recorded using a JASCO FT/IR-4200 (Jasco Inc., Japan) spectrometer. OS lignin residues (OSL-40, OSL-30, and OSL-15) were dispersed in KBr to obtain disks which were placed in a holder. Dispersions of OS

lignin residues in ELO were directly deposited in an appropriate sample holder. The spectra were collected in the transmission mode at 4 cm^{-1} resolution.

Nuclear Magnetic Resonance (NMR) Analysis

^{13}C–^{1}H two-dimensional nuclear magnetic resonance (2D NMR) analysis of OS lignin residues (OSL-40, OSL-30, and OSL-15), ELO and dispersions of OS lignin residues in ELO [dissolved in deuterated dimethylsulfoxide, DMSO-d_6 (0.75 mL)] was adquired at 25 °C in a Bruker Avance III 500 MHz NMR spectrometer equipped with a 5 mm BBFO plus with a z-gradient double-resonance probe. HSQC (heteronuclear single quantum correlation) experiment was recorded according to previously reported operation conditions [21]: spectral widths, 8196.72 Hz for the ^{1}H dimensions, and 163,868 Hz for ^{13}C dimensions (20,754.50 for dispersions of OS lignin residues in ELO); number of collected complex points, 1024 for 1H-dimension with a recycle delay of 1 s; scans number 32; time increments (^{13}C) 256; 1 JC-H (Hz): 145; J-coupling evolution delay set to 3.45 ms; squared cosine-bell apodization function applied in both dimensions. Residual DMSO (from DMSO-d_6) was employed as an internal reference (δ_C/δ_H 39.6/2.5 ppm) [21]. In addition, ^{1}H and ^{13}C NMR analyses were also carried out for ELO and dispersions of OS lignin residues in ELO, using the same spectrometer. ^{1}H NMR experiments were carried out under the following operation conditions: pulse 90° (μs) 6.238; recycle delay (s) 10; spectral width (Hz) 9615.38; acquisition time (s) 3.4; scans number 32. ^{13}C NMR experiments were carried out under the following operation conditions: pulse 30° (μs) 3.3; recycle delay (s) 2; spectral width (Hz) 30,120; acquisition time (s) 1.09; scans number 9165.

Size Exclusion Chromatography (SEC) Analysis

Weight-average (Mw), number-average (Mn) molecular weights, and polydispersity (Mw/Mn)) of OS lignin residues (OSL-40, OSL-30, and OSL-15) were obtained from SEC analysis performed by HPLC (1260 HPLC, Agilent, Waldbronn, Germany), equipped with a G1315D diode array detector. GPC P4000 and P5000 columns, both 300 × 7.8 mm, coupled in series and a safeguard column, 35 × 7.8 mm, (Phenomenex) were employed using NaOH (0.05 M) as a mobile phase (1 mL min^{-1} at 25 °C for 30 min). The samples were measured at 254 nm. Polystyrene sulfonated standards (peak average molecular weights of 4210, 9740, 65,400, 470,000, PSS-Polymer Standards Service) were employed for calibration.

Thermogravimetric Analysis (TGA)

Mass loss versus temperature curves was recorded under N_2 purge in a thermogravimetric analyser Q-50 (TA Instruments, Newcastle, USA). OS lignin residues (OSL-40, OSL-30, and OSL-15) and ELO were placed on platinum pans and heated from 30 to 600 °C, at 10 °C/min.

Rheological Characterization

Viscous flow curves of both ELO and OS lignin residues dispersions in ELO were obtained in a controlled-stress rheometer (Haake RheoScope, Thermo Fisher Scientific, Germany), at 25 °C, using a plate-plate geometry (35 mm diameter, 1 mm gap). Small amplitude oscillatory shear (SAOS) tests were performed on OSL-40-ELO, OSL-30-ELO, and OSL-15-ELO thickened formulations inside the linear viscoelastic region, in a frequency range of 0.03–100 rad/s, at 25 °C.

Results and Discussion

Chemical Composition of OS Lignin Rich-Residues

Table 1 displays the chemical composition of OS lignin residues after a fractionation process of OS based on acid pretreatment and a steam explosion followed by a PSSF process. As expected, the OS lignin residues showed a rather high lignin content (63.3–66.1% of acid-insoluble lignin and 3.0–3.4% of acid-soluble lignin), compared to raw olive stones (35.6% lignin). This lignin concentration is mainly due to the carbohydrates hydrolysis, solubilisation and fermentation during the sequential fractionation process and subsequent PSSF process. Acid pretreatment promotes extensive hydrolysis and solubilization of hemicelluloses [35]. Steam explosion produces an increase of the surface area and porosity and modification of the fiber structure, thus promoting a strong increase of cellulose enzymatic digestibility [35]. Finally, after pretreatments, the carbohydrates enclosed in the pretreated material are depolymerized into soluble fermentable sugars by enzymatic hydrolysis [36].

Table 1 Chemical composition (% dry weight) of olive stone lignin residues

	OSL-40	OSL-30	OSL-15
Glucan	17.4 ± 0.1	18.2 ± 0.1	19.3 ± 0.0
Xylan	2.9 ± 0.02	2.9 ± 0.0	2.8 ± 0.1
Acid soluble lignin	3.3 ± 0.8	3.4 ± 0.6	3.0 ± 0.6
Acid insoluble lignin	66.1 ± 0.4	64.5 ± 0.2	63.3 ± 0.2
TOTAL	89.7	89.0	88.4

Nonetheless, in spite of the fractionation processes and subsequent saccharification and fermentation processes, certain carbohydrate content could be still observed in the OS lignin residues, mainly glucan (17.4–19.3%) and to a lesser extent xylan (2.8–2.9%).

Similar results have been described in OS lignin residues obtained during bioethanol production from olive tree pruning (lignins recovered from steam explosion pretreatment with phosphoric acid or water as catalysts, followed by simultaneous saccharification and fermentation process) [37, 38]. The presence of carbohydrate impurities in lignin could interfere with its subsequent valorization approaches. Thus, it is essential to evaluate possible lignin valorization pathways in which the presence of these impurities does not require any additional purification processes that can rise the costs of the resulting new lignin-based products. Previous investigations have reported appropriate valorisation routes for lignins with relatively high carbohydrate contamination. For example, Borrero-López et al. [21, 22] described the viability of using OS lignin residues from steam explosion or autohydrolysis of wood and non-woody materials followed by saccharification and fermentation, as castor oil structuring agents in biolubricant formulations. In the same way, OS lignin residues derived from acid pretreatment and enzymatic hydrolysis were valorized into active carbon to be employed as electrode material in supercapacitors [39].

Structural Characterization of Both OS Lignin Residues and Formulations Resulting from Their Dispersion in Epoxidized Linseed Oil

FTIR Spectra Analysis

Figure 1a shows the FTIR spectra of OS lignin residues (OSL-40, OSL-30, and OSL-15), being the visible bands attributed according to previous studies [37, 38, 40].

Based on the chemical composition of OS lignin residues (see Table 1), FTIR spectra were dominated by characteristic lignin bands at 1600 cm^{-1}, 1511 cm^{-1}, and 1422 cm^{-1}, associated with aromatic skeleton lignin vibrations. Other lignin bands were ascribed to syringyl (S), guaiacyl (G), and p-hydroxyphenyl (H) units, including bands at 1330 cm^{-1} (S and G), 1268 cm^{-1} (G), 1216 cm^{-1} (G), 1116 cm^{-1} (S), 1030 cm^{-1} (G) and 833 cm^{-1} (S

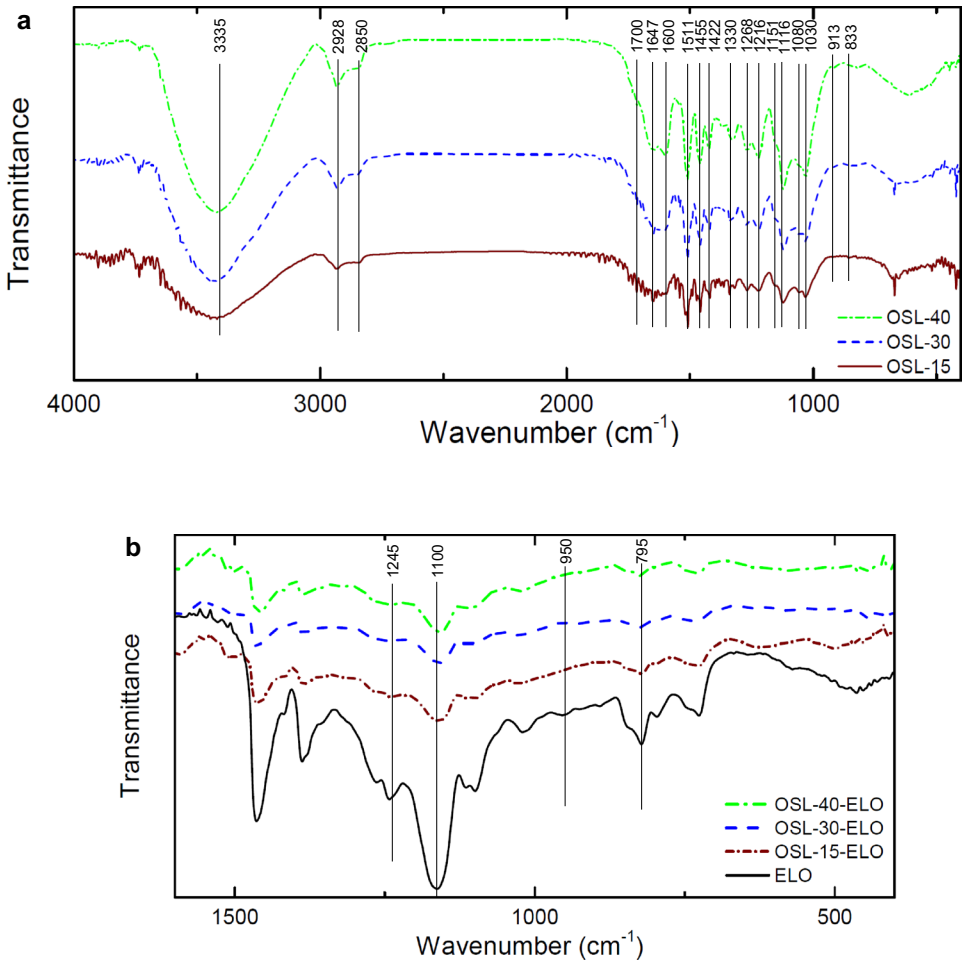

Fig. 1 FTIR spectra of OS lignin residues. **a** OSL-40 (green line), OSL-30 (blue line), and OSL-15 (brown line); and OS lignin residues dispersed in epoxidized linseed oil; **b** OSL-40-ELO (green line), OSL-30-ELO (blue line), OSL-15-ELO (brown line) and ELO (black line) (Color figure online)

and H). Moreover, all spectra showed a broad band at 3335 cm^{-1} corresponding to the O–H stretching vibration in lignin structures, either aromatic or aliphatic, as well as in carbohydrates. Similar lignin FTIR patterns were described in OS lignin residues generated during bioethanol production from olive tree pruning [37, 38].

Several bands attributed to lignin oxidation could also be detected. A slight absorption at 1700 cm^{-1} was associated with the carbonyl groups in the unconjugated ketones and ester groups stretching. Carbonyls in hemicelluloses contained in OS lignin residues could also be contributing to this absorption [41]. Conjugated C=O groups at 1647 cm^{-1} could also be found in all spectra, although this band could also be related to enzymes employed during enzymatic hydrolysis due to the presence of amide bonds [37, 38]. Finally, other bands in OS lignin residues spectra can also reveal the presence of carbohydrates contamination determined by chemical composition study (Sect. "Chemical Composition of OS Lignin Rich-Residues"). Thus, cellulose and hemicelluloses bands at 1156 cm^{-1}, 1116 cm^{-1}, and 1030 cm^{-1} are apparent, some of them overlapping lignin bands.

Formulations produced by dispersing OS lignin residues in ELO (OSL-40-ELO, OSL-30-ELO, and OSL-15-ELO) were also characterized by FTIR in order to verify intended reactions between the hydroxyl groups present in OS lignin residues, either in lignin or in carbohydrates, and the oxirane rings in ELO (Fig. 1b). A decrease, or attenuation, of the bands in the wavenumber range of 795–950 cm^{-1} of ELO, corresponding to the C–H wagging of the oxirane ring [42, 43], was observed when OS lignin residues were dispersed in it. This could indicate an opening of the epoxy rings through a possible covalent interaction with hydroxyl groups present in OS lignin residues. This epoxy rings opening was also supported by a reduction of the intensity of the bands in the wavenumber range of 1100–1245 cm^{-1}, attributed to C–O–C stretching of the oxirane ring [42]. Similar interactions between hydroxyl groups from different compounds and oxirane rings from epoxidized oils have been described in the literature. For example, Pin et al. [42] proposed the copolymerization of ELO and furfuryl alcohol through covalent bonds (ether) between the alcohol functions of furfuryl alcohol and the epoxy functions of ELO, resulting in the epoxy rings opening of ELO. Luo et al. [44] also described the inclusion of allylic double bonds into epoxidized soybean oil through an epoxy ring-opening nucleophilic incorporation of allyl alcohol, resulting in ether bonds. Finally, Lingome et al. [45] also reported the oxirane rings opening of epoxidized fatty esters (methyl or ethyl oleate) by hydroxyl groups from alkyl glycosides leading to the formation of hydroxyalkyl ethers.

NMR Spectra Analysis

Fig. S1 shows the 2D NMR HSQC whole spectra of OS lignin residues (OSL-40, OSL-30, and OSL-15, respectively), whereas Fig. 2 displays the spectra assigned to the oxygenated aliphatic and the aromatic regions. The ^{13}C–^{1}H lignin correlation signals found in HSQC spectra are displayed in Table 2, attributed according to those identified by different authors [37, 38, 40, 46, 47]. The lignin substructures and carbohydrates found are illustrated in Fig. 3.

The oxygenated aliphatic region of OS lignin residues spectra gives evidence of the different inter-unit linkages existing in OS lignin (Fig. 2a, c and e). In general, β-O-4′ alkyl aryl ethers signals [C_α–H_α for β-O-4′ G and S lignin units (A_α), C_β–H_β for β-O-4′ G and S units (A_β), and C_γ–H_γ (A_γ)] could be identified indistinctly in all spectra. Signals from C–C linkages, such as β–β′ resinol (B) and β-5′ phenylcoumaran (C) substructures, were also readily observed. They comprised correlation signals of C_α–H_α (B_α), C_β–H_β (B_β) and the double C_γ–H_γ (B_γ) in the case of β–β′ resinol; and C_α–H_α for G and S lignin units (C_α), C_β–H_β for S units (C_β), and C_γ–H_γ (C_γ) for β-5′ phenylcoumaran. C_α–H_α (E_α) and $C_{\alpha'}$–$H_{\alpha'}$ ($E_{\alpha'}$) signals for spirodienones and C_γ–H_γ signal for cinnamyl alcohol end-groups (I_γ) were also visible in all lignin spectra. These groups of substructures and end groups found in OS lignin have already been reported in native lignin from olive tree pruning [47], as well as in lignin residues produced in an olive tree pruning-based biorefinery (i.e., alkaline pulping and bioethanol production) [37, 38, 40].

The aliphatic-oxygenated region of OS lignin residues also revealed carbohydrates signals (Fig. S1a, b and c; and Fig. 2a, c and e), either from hexose or pentose units, according to the chemical composition previously determined (Table 1). These signals included mainly correlations (X_2, X_3, X_4, and X_5) of the xylan chain. Moreover, the C-1 cross signal for (1–4) β-D-Xylp of xylan and β-D-Gluc of glucan and α- and β-xylose reducing ends were also found (Fig. S1a, b and c).

In the aromatic region of OS lignin residues spectra, the characteristic correlation signals of S, G, and H lignin units were seen (Fig. 2b, d and f). The S lignin units displayed correlations of $C_{2,6}$–$H_{2,6}$ ($S_{2,6}$). The G lignin units showed correlations for C_2–H_2 (G_2), C_5–H_5 (G_5), and C_6–H_6 (G_6); whereas the H lignin units presented correlations of $C_{2,6}$–$H_{2,6}$ ($H_{2,6}$) and $C_{3,5}$–$H_{3,5}$ ($H_{3,5}$). Moreover, several correlation signals attributed to lignin oxidation could also be observed. They included syringaldehyde or acetosyringone ($S'_{2,6}$), vanillin (G'_2 and G'_6), and acetovanillone (G''_2 and G''_6). Lastly, other native lignin units attributed to $C_{2,6}$–$H_{2,6}$ ($J_{2,6}$) of cinnamaldehyde end-groups in S units (sinapaldehyde end-groups) and C_6–H_6 (J_6) in G units (coniferaldehyde

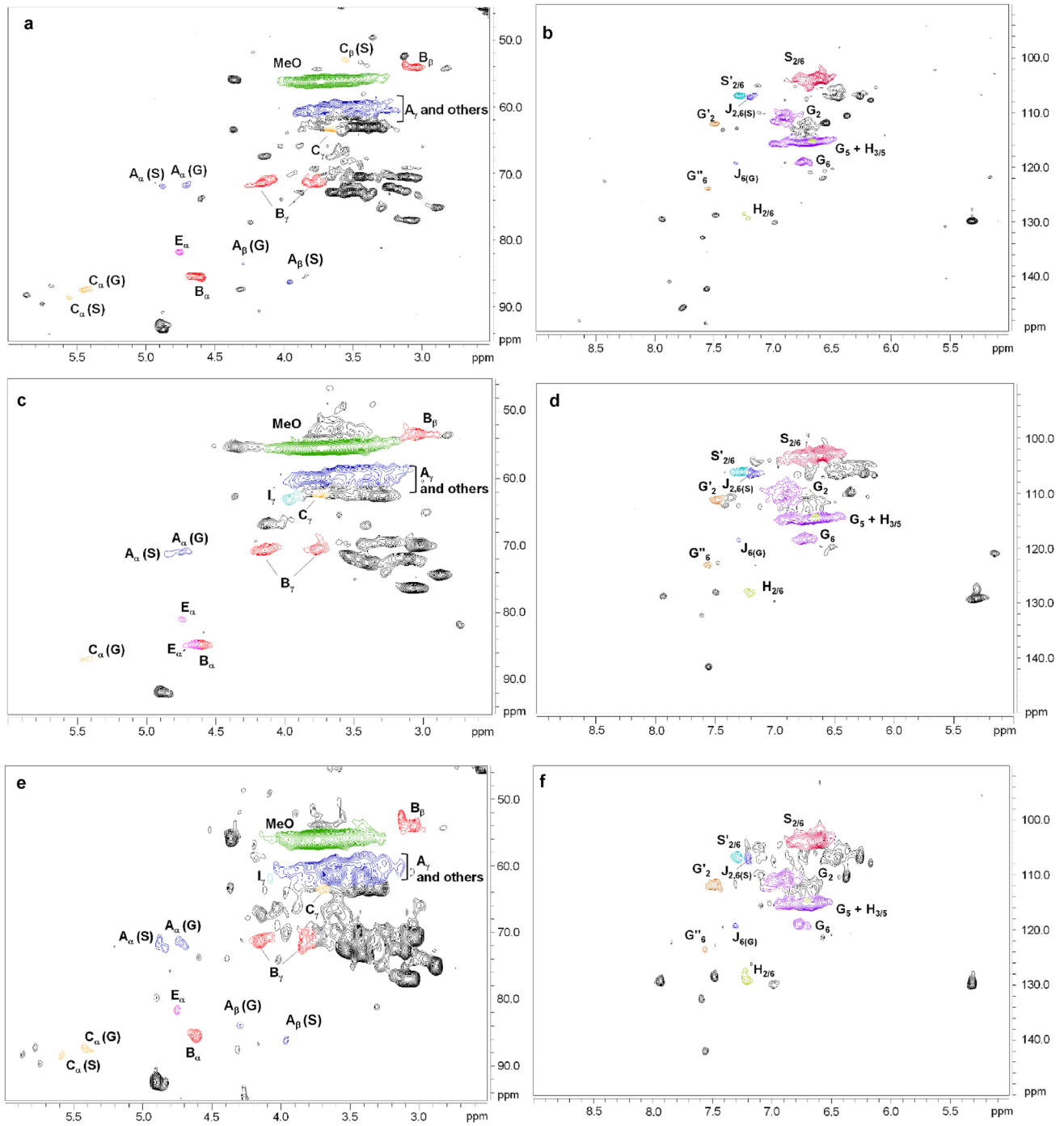

Fig. 2. 2D NMR HSQC spectra of OS lignin residues. Aliphatic oxygenated region (δ_C/δ_H 45.0–95.0/2.5–6.0 ppm) and aromatic region (δ_C/δ_H 90.0–150.0/5.0–9.0 ppm). OSL-40 (**a** and **b**), OSL-30 (**c** and **d**), and OSL-15 (**e** and **f**)

end-groups), previously described in lignin from olive tree pruning [40, 47], could also be identified in lignin from OS.

Relative percentages of the total inter-unit linkages, end groups referred to the total side-chains, aromatic units and S/G ratios are displayed in Table 3. In general, OS lignin residues showed a predominance of β–β′ resinol substructures (59.0% for OSL-40, 53.9% OSL-30, and 51.0% for OSL-15), followed by β-O-4′ alkyl aryl ethers (27.0% for OSL-40, 34.2% OSL-30, and 35.2% for OSL-15), and β-5′ phenylcoumaran substructures (13.2% for OSL-40, 9.2% OSL-30, and 11.4% for OSL-15). Lower proportions of spirodienones and cinnamyl alcohol end-groups were also determined. With regard to the aromatic region of OS

Table 2 Assignment of main lignin and carbohydrates ^{13}C–^{1}H correlation peaks in the 2D NMR HSQC spectra of OS lignin residues

δ_C/δ_H (ppm)	Assignment
53.5/3.49	C_β–H_β, phenylcoumaran substructures **S** units (**C**)
54.0/3.04	C_β–H_β, resinol substructures (**B**)
56.1/3.71	C–H, methoxyls (**MeO**)
60.6/3.37–3.63	C_γ–H_γ, *β-O*-4′ substructures (**A**)
61.9/4.07	C_γ–H_γ, cinnamyl alcohol end groups (**I**)
62.7/3.65	C_γ–H_γ, phenylcoumaran substructures (**C**)
63.2/3.21–3.89	C_5–H_5, xylan
71.3/3.76–4.18	C_γ–H_γ, resinol substructures (**B**)
71.5/4.78	C_α–H_α, β-O-4′ **G** unit (**A**)
72.1/4.87	C_α–H_α, β-O-4′ **S** unit (**A**)
72.7/3.07	C_2–H_2, xylan
74.0/3.26	C_3–H_3, xylan
75.7/3.54	C_4–H_4, xylan
81.6/4.72	C_α–H_α, spirodienone substructures (**E**)
83.8/4.28	C_β–H_β, β–O–4′ (**G**) unit **A**
85.3/4.74	$C_{\alpha'}$–$H_{\alpha'}$, spirodienone substructures (**E**)
85.5/4.63	C_α–H_α, resinol substructures (**B**)
86.3/4.04	C_β–H_β, β–O–4′ (**S**) unit **A**
87.5/5.42	C_α–H_α, phenylcoumaran substructures **G** units (**C**)
88.5/5.59	C_α–H_α, phenylcoumaran substructures **S** units (**C**)
92.3/4.89	reducing end (1–4) α-D-Xylp
97.3/4.27	reducing end (1–4) β-D-Xylp
101.6/4.30	C-1, (1–4) β-D-Xylp
103.8/4.13	C-1, (1–4) β-D-Glcp
104.3/6.69	$C_{2,6}$–$H_{2,6}$, S units (**S**)
106.2/7.12	$C_{2,6}$–$H_{2,6}$, in cinamaldehyde end-groups **S** units (**J**)
106.6/7.31	$C_{2,6}$–$H_{2,6}$, oxidized (H–C_α=O or H_3C–C_α=O) S units (**S′**)
111.0/6.88	C_2–H_2, G units (**G**)
111.0/7.37	C_2–H_2, oxidized (H–C_α=O) G units (**G′**)
115.0/6.74	$C_{3,5}$–$H_{3,5}$, *p*-hydroxyphenyl (**H**)
115.2/6.42–6.81	C_5–H_5, G units (**G**)
119.4/7.30	C_6–H_6, in cinamaldehyde end-groups **G** units (**J**)
119.6/6.78	C_6–H_6, G units (**G**)
123.6/7.51	C_6–H_6, oxidized (H_3C–C_α=O) G units (**G″**)
128.3/7.19	$C_{2,6}$–$H_{2,6}$, *p*-hydroxyphenyl (**H**)

lignins, the S/G ratios calculated by 2D-NMR were 1.5 for OSL-40, 1.3 for OSL-30, and 1.2 for OSL-15.

It is well known that native lignin suffers different transformations under the pretreatment processes used herein, i.e., acid hydrolysis and steam explosion [48, 49]. The external acid catalyst (i.e., sulphuric acid) added during acid pretreatment as well as the organic acids (i.e., acetic and uronic acids) generated under both pretreatment steps lead to acid-based cleavage of β-O-4′ alkyl aryl ethers. It can explain the lower β-O-4′ alkyl aryl ethers linkages content quantified for olive stone lignins compared to other substructures such as β–β′ resinol, the majority substructure found in these lignins. Santos et al. [37] have already described a β-O-4′ alkyl aryl ethers breakdown in lignin from olive tree pruning residue during steam explosion pretreatment, an effect which was increased when the steam explosion was carried out under acidic conditions [38]. Even, the following enzymatic hydrolysis of pretreated materials continues generating acetates due to certain activities, such as xylanase present in the enzymatic cocktails such as Cellic®CTec. Then, these acetates can act on lignin, modifying its structure via β-O-4 linkage acidic breakdown [50, 51]. This could describe the lower β-O-4′ content in OSL-40 lignin (27.0%), a residual sample generated from pretreated material hydrolyze with 40 FPU of Cellic® CTec2/g of dry substrate, compared to OSL-30 (34.2%) or OSL-15 (35.2%) lignins produced from pretreated materials hydrolysed with 30 or 15 FPU of Cellic® CTec2/g of dry substrate, respectively. Moreover, the higher β-O-4′ depolymerization observed at higher hydrolytic enzyme dosages let to a slightly higher phenolic groups content (55.0 ± 2.3 mg GAE/g lignin for OSL-40; 49.0 ± 4.8 mg GAE/g lignin for OSL-30; and 48.0 ± 4.9 mg GAE/g lignin for OSL-15) (Table S2).

Degradation of β–β′ resinol, β-5′ phenylcoumaran, and spirodienones substructures has been also described in lignins of different materials pretreated with acid hydrolysis and steam explosion processes [49, 51], including lignin from olive tree pruning residue [37, 38]. By contrast, other authors have described an increase in the amount of some of these substructures. In this sense, Rahikainen et al. [52] and Heikkinen et al. [50] reported an increment in the abundance of β-5′ phenylcoumaran as a consequence of a rearrangement between interunit linkages, with an initial homolytic breakdown of the β-O-4′ and a subsequent generation of the new β-5′ linkages [53].

Regarding S/G ratios, the values observed for OS lignin residues are lower compared to lignins from side-streams recovered from black liquors from alkaline cellulosic pulp production of olive tree pruning (S/G ratios around 5) [38, 40], due to the preferential solubilization of S units during alkaline pulping. Regarding acid pretreatment, an increase of S units of solubilized lignin is also produced due to a favored release of S units into the aqueous phase [54]. Similarly, steam explosion is also associated to an initial preferential removal of S units at short autohydrolysis or steam explosion times. In this sense, Rahikainen et al. [52] and Heikkinen et al. [50] reported a considerable reduction in the S/G ratio of the lignin (insoluble residue) after the steam explosion treatment of wheat straw. Then, taking into account the preferential solubilization of S units during acid and steam explosion pretreatment of OS, lignin residues showed S/G ratios with low values.

The dispersion of the OS lignin residues in ELO was also evaluated by ^{1}H and ^{13}C NMR analysis (Figs. 4 and

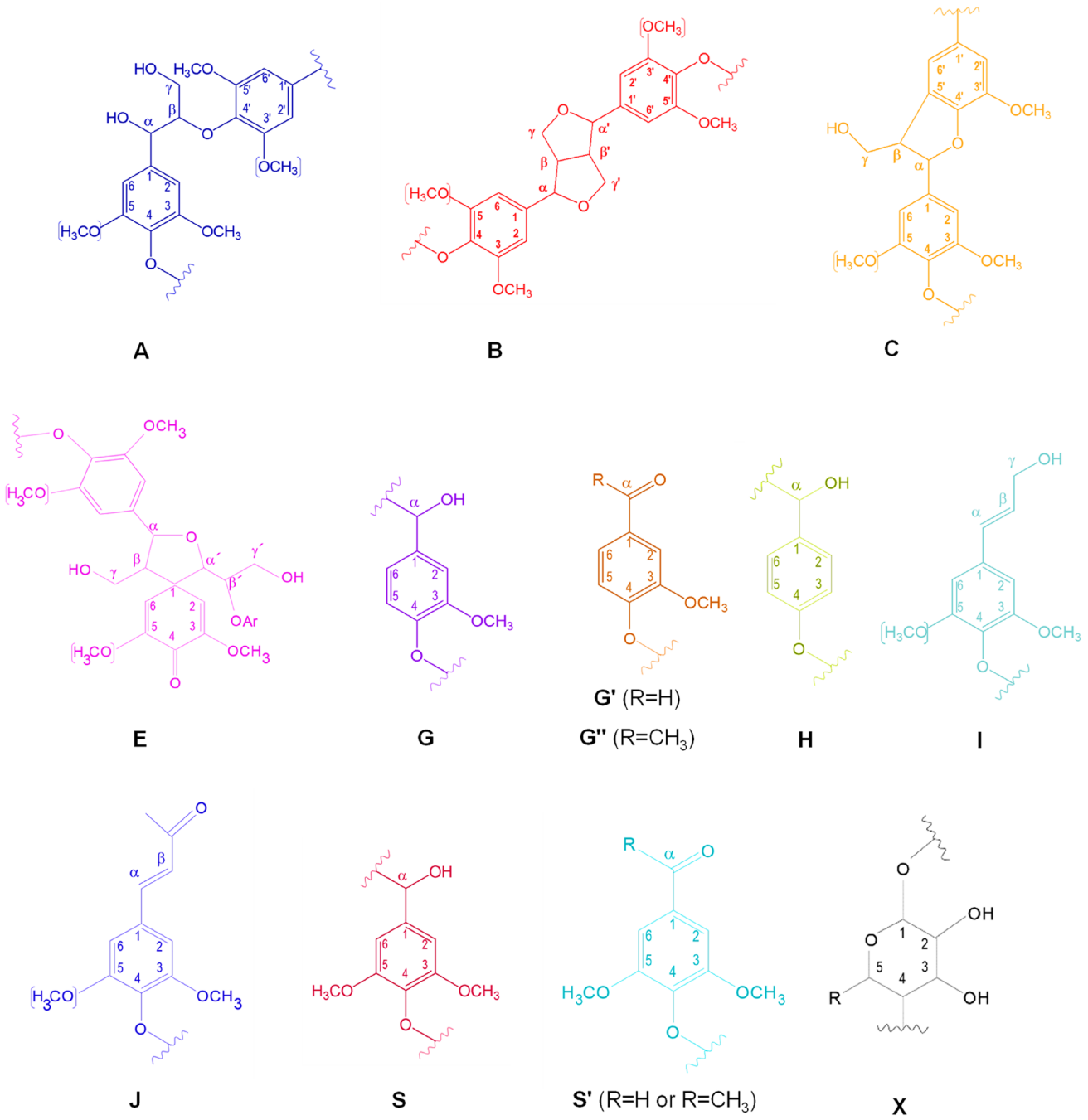

Fig. 3 Main lignin and carbohydrate substructures identified in aliphatic oxygenated and aromatic regions of OS lignin residues: **A**, β-O-4′ alkyl-aryl ether; **B**, β–β′ resinols; **C**, β-5′ phenylcoumarans; **E**, spirodienones; **G**, guaiacyl unit; **G′**, vanillin; **G″**, acetovanillone; **H**, p-hydroxyphenyl unit; **I**, cinnamylalcohol end-groups; **J**, cinnamyl aldehyde end-groups; **S**, syringyl unit; **S′**, syringaldehyde or acetosyringone; **X**, xylopyranose (R, OH)

5, respectively), as well as by 2D NMR HSQC (Fig. S2). The aim was to corroborate the possible chemical reaction observed by FTIR analysis (Sect. "Structural Characterization of Both OS Lignin Residues and Formulations Resulting from Their Dispersion in Epoxidized Linseed Oil") between hydroxyl groups present in OS lignin residues and oxirane rings of ELO. Considering the ELO structure (Fig. 4a), major modifications arise in ^{1}H NMR spectrum when OS lignin residues were dispersed in it (Fig. 4b). As can be seen, the peaks attributed to protons of the oxirane ring at δ_H 3.1 and 2.8 ppm, of the methylene bridge between two epoxy rings, δ_H 1.8 ppm, and of the methylene next

Table 3 Relative percentages of the total inter-unit linkages, end groups referred to the total side-chains, aromatic units and S/G ratios of OS lignin residues

	OSL-40	OSL-30	OSL-15
Lignin interunit linkages (%)			
β-O-4′ (**A**)	27.0	34.2	35.2
Resinols (**B**)	59.0	53.9	51.0
Phenylcoumarans (**C**)	13.2	9.2	11.4
Spirodienones (**E**)	0.8	2.7	2.4
Lignin end-groups[a]			
Cinnamyl alcohol end-groups (**I**)	–	3.0	4.0
Lignin aromatic units[b]			
H (%)	4.4	2.2	3.4
G (%)	38.4	42.2	43.4
S (%)	57.2	55.6	53.2
S/G ratio	1.5	1.3	1.2

A semi-quantitative analysis of lignin units and linkages, based on measuring the contour volume integrals of correlation signals, was performed according to Rencoret et al. [47]. Then, abundance of β-O-4′, resinols, phenylcoumaran, and spirodienones substructures was calculated by 2D NMR from C_α–H_α correlations. Cinnamyl alcohol end-groups using C_γ–H_γ correlations; $C_{2,6}$–$H_{2,6}$ correlations from S units; and C_2–H_2 correlations from G units were employed to calculate the S/G lignin ratios

[a]Expressed as a fraction of the total lignin interunit linkage types A–E

[b]Molar percentages (H + G + S = 100)

to the oxirane ring, δ_H 1.5 ppm [42, 43], became broader or disappeared. In addition, a new broad peak between δ_H 3.2–3.9 ppm was observed in the resulting dispersion of the OSL-40-ELO sample (Fig. 4b). This new peak, apart from the methoxy groups in lignin, could also correspond to protons attached to carbon and oxygen of –CHOH groups [55]. These observations were also described during cross-linking of epoxidized linseed oil and aliphatic/aromatic diacids [43], copolymerization of epoxidized linseed oil with furfuryl alcohol [42] and epoxidized soybean oil and allyl alcohol [56]. They highlight the opening of epoxides groups of ELO, corroborating the possible covalent interaction of them with hydroxyl groups from OS lignin residues, previously described by FTIR. ^{13}C NMR also supported the opening of epoxides groups (Fig. 5), showing a decrease of the –CH– resonance at δ_C 53–58 ppm from the oxirane ring when OS lignin residues were dispersed in ELO [42]. Finally, 2D NMR HSQC experiments of formulations produced from OS lignin residues dispersed in ELO supported the observations found by ^1H and ^{13}C NMR analysis. Compared to the ELO spectrum (Fig. S2a), new peaks appeared in the range of δ_C/δ_H 70.0–85.0/3.00–4.5 ppm corresponding to secondary alcohol and methylene ether (Fig. S2b), confirming the oxirane rings opening of ELO by hydroxyls groups of OS lignin residues. Licsandru et al. [57] also described these signals in 2D NMR HSQC spectra when hydroxyl functions of humins reacted with oxirane rings of ELO.

SEC Analysis

Fig. S3 displays the molecular weight distribution of OS lignin residues (OSL-40, OSL-30, and OSL-15), displaying several fractions well-distinguished; one showing a higher molecular weight broad peak, and others showing lower molecular weight narrow peaks. High weight-average molecular values Mw were obtained from molecular weight distribution (22,000–25900 Da) (Table 4). In general, lignins remaining in the residues from enzymatic hydrolysis of pretreated materials usually show higher molecular weight values compared to lignins solubilized during the pretreatment step [21, 58]. As previously mentioned, acid-based cleavage of β-O-4′ alkyl aryl ethers is produced during both acid and steam explosion pretreatments, leading to lignin depolymerization and, consequently a decrease in molecular weight. Nevertheless, polymerization reactions can also take place under acidic conditions [48], mainly via C–C bonds, giving increments in Mw values [59]. The high polydispersity values observed for OS lignin residues (between 13.2 and 11.8), could confirm that polymerization reactions have taken place during both acid and steam explosion pretreatments [60]. Nevertheless, the high Mw of the OS lignins could be also attributed to the presence of carbohydrates in the OS lignin residues (Sect. "Chemical Composition of OS Lignin Rich-Residues"), as during the preparation of these residues for SEC analysis, an alkaline solubilisation of carbohydrates could take place, remaining them covalently link to the lignins [61]. High molecular weights were also reported by Dávila et al. [62] in lignin residues obtained from vine shoots during autohydrolysis pretreatment and subsequent simultaneous saccharification and ethanol fermentation.

Thermal Analysis

The thermal degradation curves in the form of both weight loss and rate of weight loss (first derivative) of the different OS lignin residues (OSL-40, OSL-30, and OSL-15) are shown in Fig. 6. Regarding the chemical composition (Sect. "Chemical Composition of OS Lignin Rich-Residues"), besides the small initial weight loss due to the residual moisture content of the samples, the dehydration of the different hydroxyl groups present in the chemical structure of lignocellulosic components (hydrogen bonds and C–OH linkages) takes place at around 150 °C [63]. This peak seems to be more relevant for OSL-40 and OSL-30, which could be explained by attending the total lignin content of both samples as well as their higher degradation, comprising a higher number of hydroxyls [26], as described in NMR section.

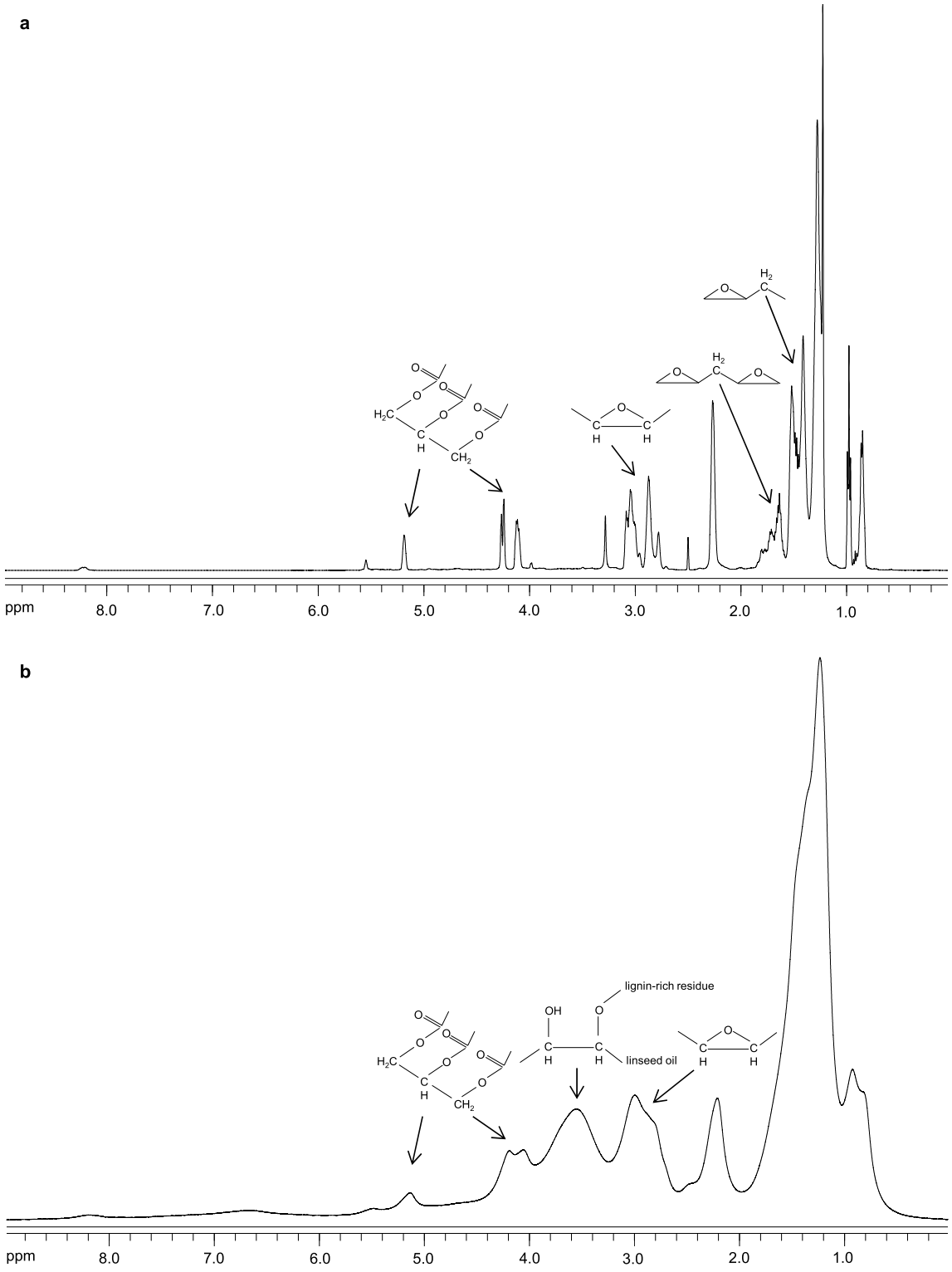

Fig. 4. ^{1}H NMR spectra of **a** epoxidized linseed oil (ELO) and **b** formulation obtained from OS lignin residues dispersed in ELO

Moreover, at 250 °C, another thermal event appeared as a slight shoulder, which can be assigned to the ether linkages cleavage, being more noticeable for OSL-15 and OSL-30 lignin residues involving higher quantities of glucan [64, 65]. This also verifies the lower β-O-4′ content in the OSL-40 sample as a consequence of the enzymatic hydrolysis

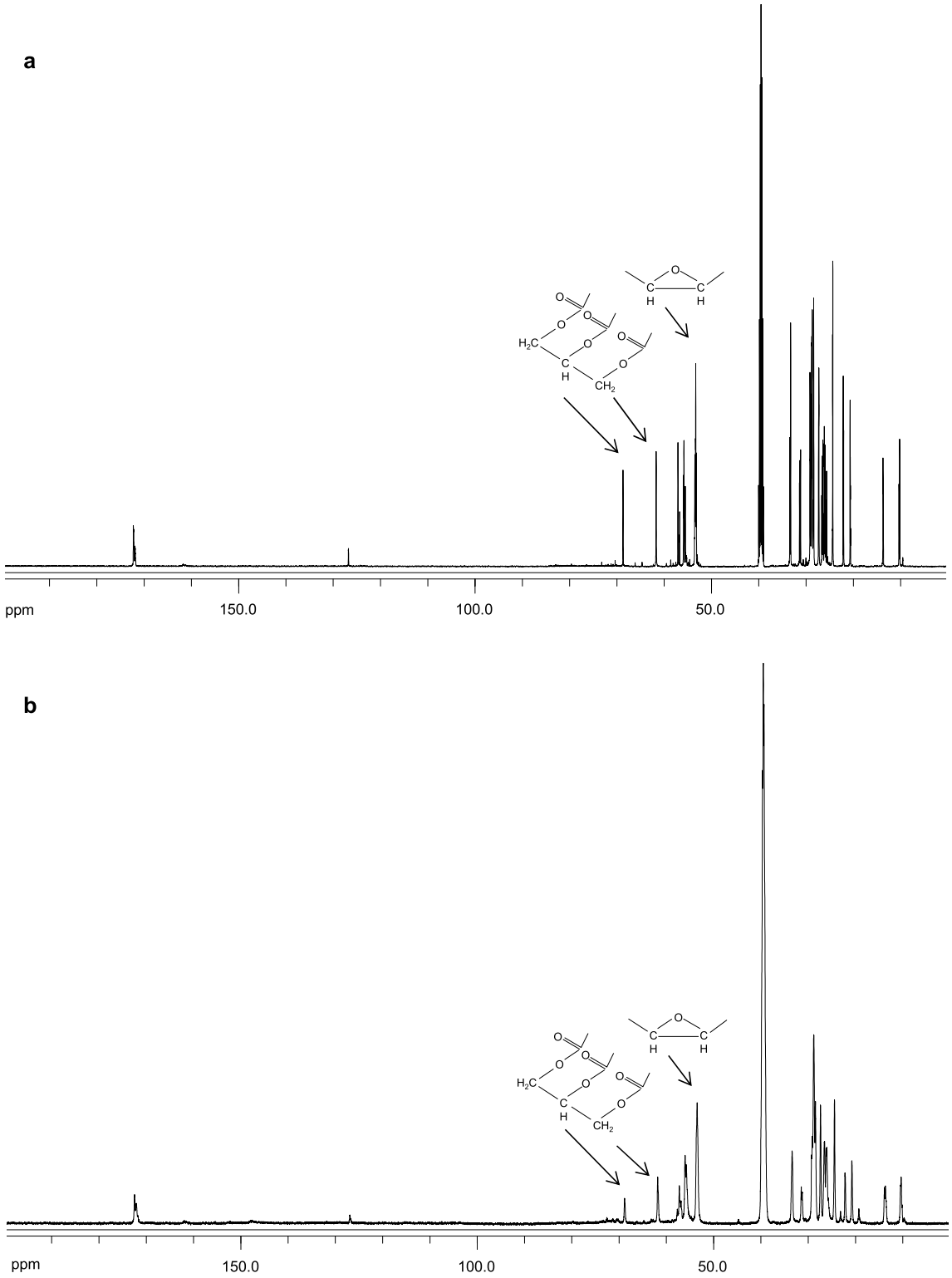

Fig. 5. ^{13}C NMR spectra of **a** epoxidized linseed oil (ELO) and **b** formulation obtained from OS lignin residues dispersed in ELO

treatment of pretreated materials, as shown in Table 3. The thermal degradation of ether units generates different volatile gases like CO, CO_2, and CH_4, among others, promoting pyrolytic processes that include the rupture of carbon–carbon linkages of both the lignin aromatic structures and cellulose skeleton at high temperatures (at around 340 °C).

Table 4 Weight average (*Mw*) and number-average (*Mn*) molecular weights and polidispersity (*Mw/Mn*) of OS lignin residues

	OSL-40	OSL-30	OSL-15
Mw	22,400	25,885	22,065
Mn	1850	1965	1870
Mw/Mn	12.1	13.2	11.8

Mw and Mn are given in Da

As can be noticed, this thermal stage begins earlier for the OSL-40 sample as a consequence of the higher quantity of the total lignin content, which is verified by means of the β–β′ resinol, β-5′ phenylcoumaran, and spirodienones substructures comprising the cited lignin residue. At this temperature, free radicals are usually formed, starting the depolymerization of these lignin-based residues and giving rise to further polymerization reactions (at around 400 °C) with the subsequent char formation [63].

Rheological Characterization of OS Lignin Residues in Epoxidized Linseed Oil

The OS lignin residues were dispersed in ELO to obtain thickened formulations. As previously reported for similar systems [17], physical stabilization and thickening were attained by means of chemical crosslinking between the epoxy groups that form the chemical structure of ELO and the hydroxyl groups contained in the OS lignin residues. Conversely, blends of unmodified vegetable oils and lignin gave rise to unstable suspensions [26]. This fact corroborates the intended chemical reaction promoted by covalent interactions between ELO and OS lignin residues, as previously observed in NMR and FTIR analyses. Figure 7 shows the viscous flow curves of both ELO and the resulting thickened formulations, prepared by adding 30 wt% of the three OS lignin residues. A noticeable increase in viscosity (over tenfold increments) in relation to ELO's viscosity can be observed in the three samples thickened with the OS lignin residues. Moreover, ELO exhibited a Newtonian behavior, as similarly found in other epoxidized oils [66, 67] while a shear-thinning response was evinced in the lignin-thickened dispersions. These flow curves were satisfactorily fitted to the power-law model (see inset in Fig. 7), which describes the shear-thinning flow behavior observed within the shear range analyzed, being K and n the consistency and flow indexes, respectively. As can be seen, flow index values lower than 1 were obtained for all OSL-containing samples, thus modifying the Newtonian characteristics of pure oils, which is indicative of a certain structuration level. On the other hand, an almost identical viscous flow response can be observed for the three lignin dispersions, regardless of the hydrolytic enzyme dose used during presaccharification. This result is somewhat expected considering that the composition and chemical structure of the three OS lignin residues are not very different, as previously discussed.

Figure 8 displays the mechanical spectra acquired from SAOS measurements inside the linear viscoelastic range (see the stress sweep experiments in Fig. S4) for the thickened formulations based on OS lignin residues and ELO at 30 wt% concentration. Again, as can be observed, the linear viscoelastic response is qualitatively comparable for

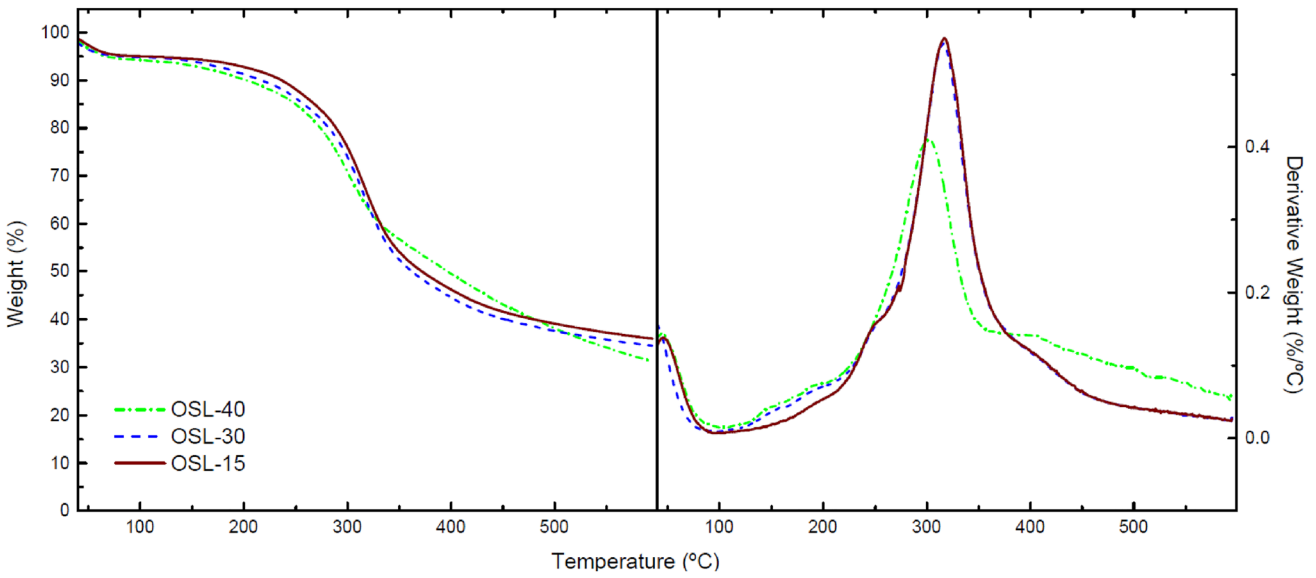

Fig. 6 Thermal degradation curves of OS lignin residues. OSL-40 (green line), OSL-30 (blue line), and OSL-15 (brown line) (Color figure online)

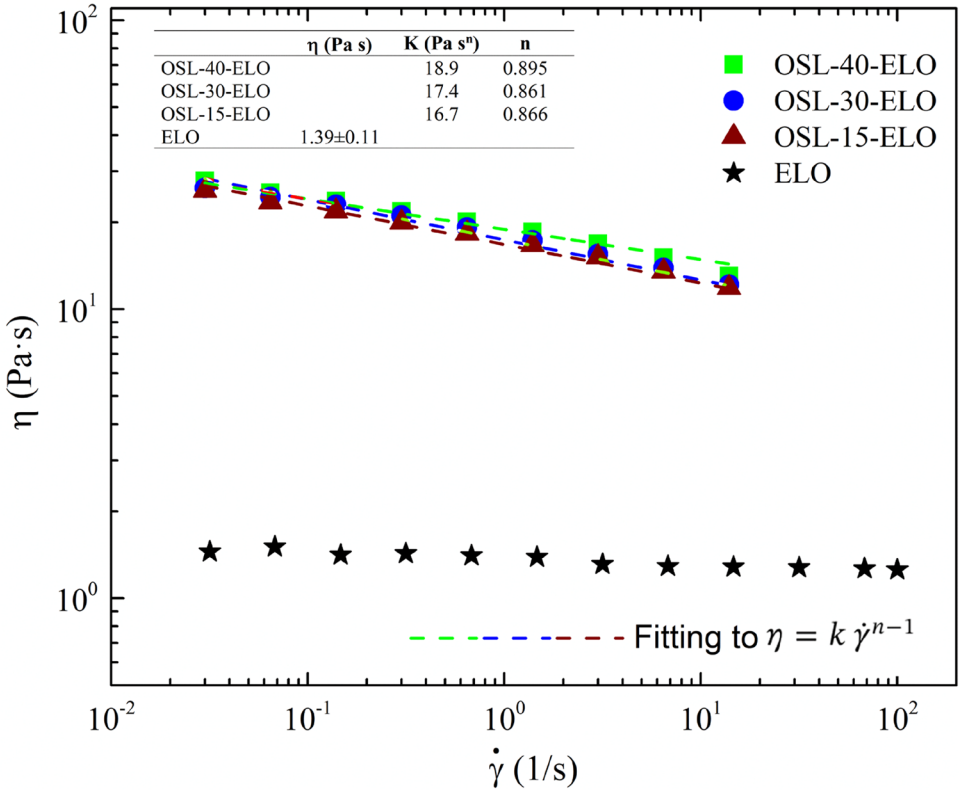

Fig. 7 Viscous flow curves of both raw material (ELO) and lignin-thickened formulations (30 wt%) as a function of OS lignin residues

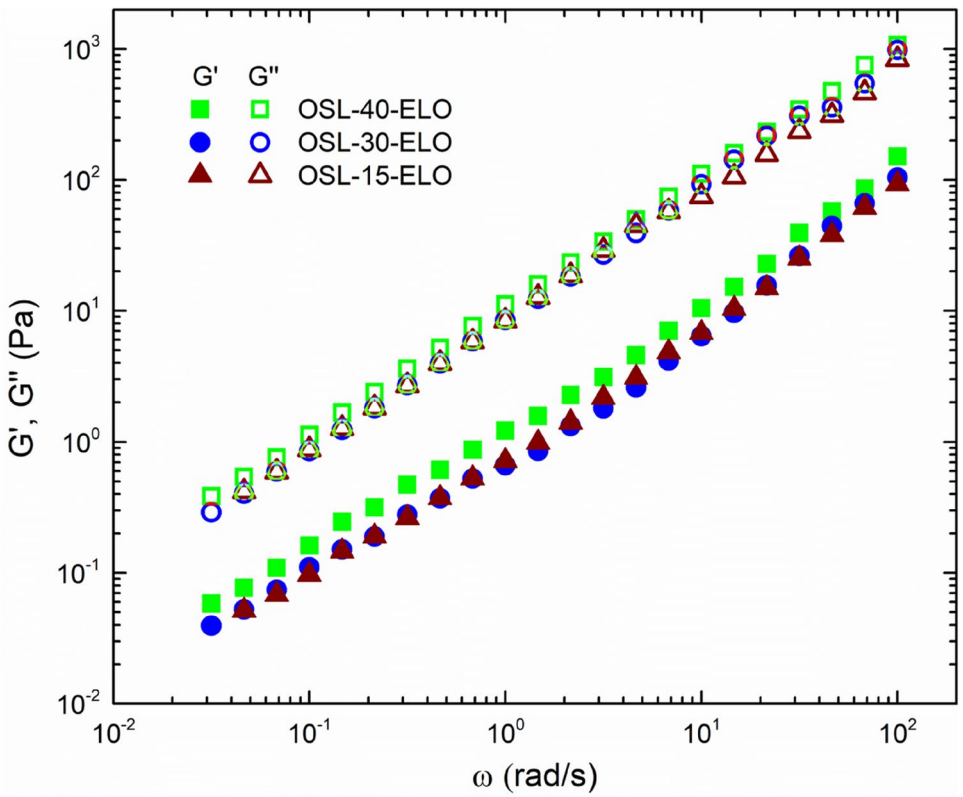

Fig. 8 Frequency dependence of the storage, G′, and loss, G″, moduli for thickened formulations based on OS lignin residues and ELO

all the formulations analyzed in the whole frequency range studied. The mechanical spectra reveal a rheological behavior that corresponds to viscoelastic liquids, where the loss modulus (G″) is around one decade higher than the storage modulus (G′). However, the evolution of both moduli with frequency deviates from the typical response of pure liquids in the terminal flow region, i.e., $G' \sim \omega^2$ and $G''(\omega) \sim \omega$. In this case, both moduli evolve with the frequency almost in parallel and proportional to $\omega^{0.9-1}$, again indicating oil structuration to some extent. A very similar frequency dependence was obtained for dispersions of a lignin fraction from sugarcane bagasse residue in a highly epoxidized castor oil [17]. Despite the very similar viscoelastic responses found for the three OS lignin residues, slightly higher values of both SAOS functions, especially G′, can be appreciated for sample OSL-40-ELO, i.e. higher relative elasticity, probably due to the higher total lignin content found in OSL-40 sample. Moreover, the lignin contained in this sample showed a lower amount of β-O-4′ substructures and, consequently more phenolic groups available (Table S2) to react with the epoxy groups.

Conclusions

OS were subjected to a sequential acid/steam explosion pretreatment followed by pre-saccharification, with different enzyme dosages, and simultaneous saccharification and ethanol fermentation (PSSF). The resulting OS lignin residues presented high lignin content, together with some carbohydrate impurities, values that depended on the hydrolytic enzyme dosages used (lower carbohydrate contents at higher hydrolytic enzyme dosages used). Moreover, the lignins contained in OS lignin residues displayed a well-maintained structure, despite the different depolymerization reactions produced during pretreatment and subsequent PSSF stages. Then, the main inter-unit linkages such as β–β′ resinol, β-O-4′ alkyl aryl ethers, and β-5′ phenylcoumaran substructures could be detected, together with high molecular weight, and low S/G ratio and phenolic groups content. Nevertheless, at higher hydrolytic enzyme dosages used, lower C–O bonds content, lower molecular weight and higher phenolic groups content were observed in OS lignin residues. Subsequently, the thickening ability of the OS lignin residues in epoxidized linseed oil (ELO) was verified, achieving viscosity increments (over tenfold increments) in relation to ELO's viscosity. Moreover, lignin-thickened formulations showed viscoelastic properties, with a frequency dependence of the storage and loss moduli that suggests oil structuration to some extent. Slightly higher relative elasticity was noticed when using OS lignin resulting from higher hydrolytic enzyme dosage. The revalorization of these OS lignin residues as oil thickeners may help to improve the profitability and sustainability of the bioethanol production process, contributing to the implementation of lignocellulosic biorefineries and, therefore to the bioeconomy development.

Supplementary Information The online version contains supplementary material available at https://doi.org/10.1007/s10924-024-03216-6.

Acknowledgements MEE and DI are grateful for the support of the Interdisciplinary Platform for Sustainable Plastics towards a Circular Economy (SusPlast-CSIC), Madrid, Spain; and Interdisciplinary Platform for Sustainability and Circular Economy (SosEcoCir-CSIC), Madrid, Spain; and Interdisciplinary Platform Horizonte Verde (CSIC), Madrid, Spain. The contribution of COST Action LignoCOST (CA17128), supported by COST (European Cooperation in Science and Technology), in promoting interaction, exchange of knowledge and collaborations in the field of lignin valorization is gratefully acknowledged.

Author contributions EC-T: Conceptualization, Investigation, Writing—review & editing; CV: Conceptualization, Investigation, Writing—review & editing, Supervision, Project administration; JMF: Conceptualization, Investigation, Writing—review & editing, Supervision, Project administration; JMO: Conceptualization, Investigation, Writing—review & editing, Supervision, Project administration; PM: Conceptualization, Investigation, Writing—review & editing, Supervision, Project administration; MEE: Conceptualization, Investigation, Writing—review & editing, Supervision, Project administration; DI: Conceptualization, Investigation, Writing—review & editing, Supervision, Project administration.

Funding Open Access funding provided thanks to the CRUE-CSIC agreement with Springer Nature. This work is collaborative research which is part of different projects: coordinated research projects (RTI2018-096080-B-C21 and RTI2018-096080-B-C22) and project PID2022-141965OB-C21 funded by MCIN/AEI/https://doi.org/10.13039/501100011033 and by "ERDF A way of making Europe", TED 2021-132122B-C1 funded by MCIN/AEI/https://doi.org/10.13039/501100011033 and by the "European UnionNextGenerationEU/PRTR", ENE2017-85819-C2-2-R funded by MINECO, and SUSTEC-CM S2018/EMT-4348 project funded by Comunidad de Madrid. The authors gratefully acknowledge the aforementioned financial support.

Declarations

Competing Interests The authors declare no competing interests.

References

1. IEA, Global Energy Review: CO2 Emissions in 2020, (n.d.). https://www.iea.org/articles/global-energy-review-co2-emissions-in-2020
2. EUROSTAT_Statistical Books. Energy, transport and environment statistics, Publications Office of the European Union, Luxembourg, 2019.
3. BP Statistical Review of World Energy 2020, (2021) 68. https://www.bp.com
4. Liu Y, Cruz-Morales P, Zargar A, Belcher MS, Pang B, Englund E, Dan Q, Yin K, Keasling JD (2021) Cell 184:1636–1647. https://doi.org/10.1016/j.cell.2021.01.052
5. Susmozas A, Martín-Sampedro R, Ibarra D, Eugenio ME, Iglesias R, Manzanares P, Moreno AD (2020) Processes 8:1310. https://doi.org/10.3390/pr8101310
6. Martínez-Patiño JC, Romero-García JM, Ruiz E, Oliva JM, Álvarez C, Romero I, Negro MJ, Castro E (2015) Energy Fuel 29:1735–1742. https://doi.org/10.1021/ef502541r
7. Romero-García JM, Susmozas A, Padilla-Rascón C, Manzanares P, Castro E, Oliva JM, Romero I (2022) Renew Energy 194:1174–1183. https://doi.org/10.1016/j.renene.2022.06.022
8. Lynd LR (2017) Nat Biotechnol 35:912–915. https://doi.org/10.1038/nbt.3976
9. Liao JJ, Latif NHA, Trache D, Brosse N, Hussin MH (2020) Int J Biol Macromol 162:985–1024. https://doi.org/10.1016/j.ijbiomac.2020.06.168
10. Ralph J, Lundquist K, Brunow G, Lu F, Kim H, Schatz PF, Marita JM, Hatfield RD, Ralph SA, Christensen JH, Boerjan W (2004) Phytochem Rev 3:29–60. https://doi.org/10.1023/B:PHYT.0000047809.65444.a4
11. Yuan T-Q, Xu F, Sun R-CJ (2013) Chem Technol Biotechnol 88:346–352. https://doi.org/10.1002/jctb.3996
12. Bajwa DS, Pourhashem G, Ullah AH, Bajwa SG (2019) Ind Crops Prod 139:111526. https://doi.org/10.1016/j.indcrop.2019.111526
13. Zoghlami A, Paës G (2019). Front Chem. https://doi.org/10.3389/fchem.2019.00874
14. Borrero-López AM, Blánquez A, Valencia C, Hernández M, Arias ME, Eugenio ME, Fillat Ú, Franco JM (2018) ACS Sust Chem Eng 6(4):5198–5205. https://doi.org/10.1021/acssuschemeng.7b04846
15. Borrero-López AM, Valencia C, Domínguez G, Eugenio ME, Franco JM (2021) Ind Crops Prod 171:113876. https://doi.org/10.1016/j.indcrop.2021.113876
16. Cortés-Triviño E, Valencia C, Delgado MA, Franco JM (2018) Carbohydr Polym 199:563–571. https://doi.org/10.1016/j.carbpol.2018.07.058
17. Cortés-Triviño E, Valencia C, Franco JM (2021) ACS Sust Chem Eng 9:10503–10512. https://doi.org/10.1021/acssuschemeng.1c02166
18. Eisen A, Bussa M, Röder H (2020) J Clean Prod 277:124277. https://doi.org/10.1016/j.jclepro.2020.124277
19. Panchal TM, Patel A, Chauhan DD, Thomas M, Patel JV (2017) Renew Sust Energ Rev 70:65–70. https://doi.org/10.1016/j.rser.2016.11.105
20. Alves FC, dos Santos VF, Monticeli FM, Ornaghi H, Barud H, Mulinari DR (2021) Polym Polym Compos 29:S1063–S1074. https://doi.org/10.1177/09673911211040360
21. Borrero-López AM, Martín-Sampedro R, Ibarra D, Valencia C, Eugenio ME, Franco JM (2020) Int J Biol Macromol 162:1398–1413. https://doi.org/10.1016/j.ijbiomac.2020.07.292
22. Borrero-López AM, Valencia C, Ibarra D, Ballesteros I, Franco JM (2022) Int J Biol Macromol 195:412–423. https://doi.org/10.1016/j.ijbiomac.2021.11.185
23. Delgado MA, Cortés-Triviño E, Valencia C, Franco JM (2020) Tribol Int 146:106231. https://doi.org/10.1016/j.triboint.2020.106231
24. Nagendramma P, Kumar P (2015) Lubricants 3:628–636. https://doi.org/10.3390/lubricants3040628
25. Jahromi H, Adhikari S, Roy P, Shelley M, Hassani E, Oh T-S (2021) ACS Sust Chem Eng 9:13424–13437. https://doi.org/10.1021/acssuschemeng.1c03523
26. Paraskar PM, Prabhudesai MS, Hatkar VM, Kulkarni RD (2021) Prog Org Coat 156:106267. https://doi.org/10.1016/j.porgcoat.2021.106267
27. Cortés-Triviño E, Valencia C, Franco JM (2017) Holzforschung 71:777–784. https://doi.org/10.1515/hf-2017-0012
28. Cecilia JA, Ballesteros Plata D, Alves Saboya R, de Luna FMT, Cavalcante CL, Rodríguez-Castellón E (2020) Processes 8:257. https://doi.org/10.3390/pr8030257
29. Gonçalves FAMM, Santos M, Cernadas T, Ferreira P, Alves P (2022) Int Mat Rev 67:119–149. https://doi.org/10.1080/09506608.2021.1915936
30. Danov SM, Kazantsev OA, Esipovich AL, Belousov AS, Rogozhin AE, Kanakov EA (2017) Catal Sci Technol 7:3659–3675. https://doi.org/10.1039/C7CY00988G
31. Santacesaria E, Tesser R, Di Serio M, Turco R, Russo V, Verde D (2011) Chem Eng J 173:198–209. https://doi.org/10.1016/j.cej.2011.05.018
32. Padilla-Rascón C, Ruiz E, Romero I, Castro E, Oliva JM, Ballesteros I, Manzanares P (2020) Ind Crops Prod 148:112279. https://doi.org/10.1016/j.indcrop.2020.112279
33. NREL, TP-510-42618 - Determination of structural carbohydrates and lignin in biomass. Chem. Anal. Test. Lab. Anal. Proced. Natl. Renew. Energy Lab., (2011)
34. Jiménez-López L, Martín-Sampedro R, Eugenio ME, Santos JI, Sixto H, Cañellas I, Ibarra D (2020) Wood Sci Technol 54:1617–1643
35. Moreno AD, Olsson L (2017) Pretreatment of lignocellulosic feedstocks in Extremophilic enzymatic processing of lignocellulosic feedstocks to bioenergy. Springer, Berlín
36. Alvira P, Ballesteros M, Negro MJ (2013) Progress on enzymatic saccharification technologies for biofuels production. In: Gupta VK, Tuohy MG (eds) Biofuel technologies: recent developments. Springer, Berlin, pp 145–169
37. Santos JI, Martín-Sampedro R, Fillat Ú, Oliva JM, Negro MJ, Ballesteros M, Eugenio ME, Ibarra D (2015) Int J Polym Sci 2015:1–11. https://doi.org/10.1155/2015/314891
38. Santos JI, Fillat Ú, Martín-Sampedro R, Eugenio ME, Negro MJ, Ballesteros I, Rodríguez A, Ibarra D (2017) Int J Biol Macromol 105:238–251. https://doi.org/10.1016/j.ijbiomac.2017.07.030
39. Martín-Sampedro R, Eugenio ME, Fillat Ú, Martín JA, Aranda P, Ruiz-Hitzky E, Ibarra D, Wicklein B (2019). Energy Technol. https://doi.org/10.1002/ente.201800685
40. Eugenio ME, Martín-Sampedro R, Santos JI, Wicklein B, Ibarra D (2021) Molecules 26:3819. https://doi.org/10.3390/molecules26133819
41. Alekhina M, Ershova O, Ebert A, Heikkinen S, Sixta H (2015) Ind Crops Prod 66:220–228. https://doi.org/10.1016/j.indcrop.2014.12.021
42. Pin J-M, Guigo N, Vincent L, Sbirrazzuoli N, Mija A (2015) Chemsuschem 8:4149–4161. https://doi.org/10.1002/cssc.201501259
43. Tran T-N, Di Mauro C, Malburet S, Graillot A, Mija A (2020) ACS Appl Bio Mater 3:7550–7561. https://doi.org/10.1021/acsabm.0c00788
44. Luo Q, Lui M, Xu Y, Ionescu M, Petrovic ZS (2013) J Appl Polym Sci 127:432–438. https://doi.org/10.1002/app.37814

45. Lingome CE, Gadenne B, Alfos C, Queneau Y, Moebs-Sanchez S (2017) Eur J Lipid Sci Technol 119:1600413. https://doi.org/10.1002/ejlt.201600413
46. Ralph, S.A., Ralph, J, Landucci, L.: Database of Lignin and cell wall model compounds, US Forest Products Laboratory, Madison, WI 2006. (2006) Available at Services/docs.htm?docids10491,access
47. Rencoret J, Gutiérrez A, Castro E, del Río JC (2018) Holzforschung 73:25–34. https://doi.org/10.1515/hf-2018-0077
48. Li J, Henriksson G, Gellerstedt G (2017) Bioresour Technol 98:3061–3068. https://doi.org/10.1016/j.biortech.2006.10.018
49. Samuel R, Foston M, Jaing N, Cao S, Allison L, Studer M, Wyman C, Ragauskas AJ (2011) Fuel 90:2836–2842. https://doi.org/10.1016/j.fuel.2011.04.021
50. Heikkinen S, Toikka MM, Karhunen PT, Kilpeläinen IA (2003) J Americ Chem Soc 125:4362–4367. https://doi.org/10.1021/ja029035k
51. Yelle DJ, Kaparaju P, Hunt CG, Hirth K, Kim H, Ralph J, Felby C (2013) BioEnerg Res 6:211–221. https://doi.org/10.1007/s12155-012-9247-6
52. Rahikainen JL, Martin-Sampedro R, Heikkinen H, Rovio S, Marjamaa K, Tamminen T, Rojas OJ, Kruus K (2013) Bioresour Technol 133:270–278. https://doi.org/10.1016/j.biortech.2013.01.075
53. Nimz H (1966) Angew Chem, Int Ed Engl 5:843–843. https://doi.org/10.1002/anie.196608431
54. Zhang L, Yan L, Wang Z, Laskar DD, Swita MS, Cort JR, Yang B (2015) Biotechnol Biofuels 8:203. https://doi.org/10.1186/s13068-015-0377-x
55. Sharma BK, Adhvaryu A, Liu Z, Erhan SZ (2006) J Amer Oil Chem Soc 83:129–136. https://doi.org/10.1007/s11746-006-1185-z
56. Wang J, Tian L, Luo B, Ramakrishna S, Kai D, Loh XJ, Yang IH, Deen GR, Mo X (2018) Colloids Surf B: Biointerfaces 169:356–365. https://doi.org/10.1016/j.colsurfb.2018.05.021
57. Licsandru E, Gaysinski M, Mija A (2020) Polymers 12:1583. https://doi.org/10.3390/polym12071583
58. Martín-Sampedro R, Santos JI, Eugenio ME, Wicklein B, Jiménez-López L, Ibarra D (2019) Int J Biol Macromol 140:3311–3322. https://doi.org/10.1016/j.ijbiomac.2019.08.029
59. Ovejero-Pérez A, Rigual V, Domínguez JC, Alonso MV, Oliet M, Rodriguez F (2020) Int J Biol Macromol 157:461–469. https://doi.org/10.1016/j.ijbiomac.2020.04.194
60. Tolbert A, Akinosho H, Khunsupat R, Naskar AK, Ragauskas AJ (2014) Biofuels Bioprod Biorefin 8:836–856. https://doi.org/10.1002/bbb.1500
61. Constant S, Wienk HLJ, Frissen AE et al (2016) Green Chem 18:2651–2665. https://doi.org/10.1039/C5GC03043A
62. Dávila I, Gullón B, Labidi J, Gullón P (2019) Renew Energy 142:612–623. https://doi.org/10.1016/j.renene.2019.04.131
63. Gul E, Al Bkoor Alrawashdeh K, Masek O, Skreiberg Ø, Corona A, Zampilli M, Wang L, Samaras P, Yang Q, Zhou H, Bartocci P, Fantozzi F (2021) J Anal Appl Pyrolysis 158:105263. https://doi.org/10.1016/j.jaap.2021.105263
64. Martín-Lara MA, Ronda A, Blázquez G, Pérez A, Calero M (2018) Process Saf Environ Protect 113:448–458. https://doi.org/10.1016/j.psep.2017.11.015
65. Trubetskaya A, Grams J, Leahy JJ, Johnson R, Gallagher P, Monaghan RFD, Kwapinska M (2020) Renew Energy 160:998–1011. https://doi.org/10.1016/j.renene.2020.06.136
66. Paul AK, Borugadda VB, Goud VV (2021) Lubricants 9:27. https://doi.org/10.3390/lubricants9030027
67. Samidin J, Salih S, Salimon N (2021) Biointerface Res Appl Chem 11:13638–13651. https://doi.org/10.33263/BRIAC115.1363813651